Absolute frequency measurement of the magnesium intercombination transition $^1S_0 \rightarrow {}^3P_1$

Jan Friebe,* André Pape, Matthias Riedmann, Karsten Moldenhauer, Tanja Mehlstäubler, Nils Rehbein, Christian Lisdat, Ernst M. Rasel, and Wolfgang Ertmer
Institute of Quantum Optics, Leibniz Universität Hannover, Welfengarten 1, 30167 Hannover, Germany

Harald Schnatz, Burghard Lipphardt, and Gesine Grosche
Physikalisch-Technische Bundesanstalt, Bundesallee 100, 38116 Braunschweig, Germany
(Received 12 September 2007; published 22 September 2008)

We report on a frequency measurement of the $(3s^2)^1S_0 \rightarrow (3s3p)^3P_1$ clock transition of ^{24}Mg on a thermal atomic beam. The intercombination transition has been referenced to a portable primary Cs frequency standard with the help of a femtosecond fiber laser frequency comb. The achieved uncertainty is 2.5×10^{-12}, which corresponds to an increase in accuracy of six orders of magnitude compared to previous results. The measured frequency value permits the calculation of several other optical transitions from $^1S_0$ to the ^3P_J-level system for ^{24}Mg, ^{25}Mg, and ^{26}Mg. We describe in detail the components of our optical frequency standard such as the stabilized spectroscopy laser, the atomic beam apparatus used for Ramsey-Bordé interferometry, and the frequency comb generator and discuss the uncertainty contributions to our measurement including the first- and second-order Doppler effect. An upper limit of 3×10^{-13} in 1 s for the short-term instability of our optical frequency standard was determined by comparison with a quartz oscillator disciplined to the signal received from the global positioning system (GPS).

DOI: 10.1103/PhysRevA.78.033830 PACS number(s): 42.62.Eh, 06.30.Ft, 37.25.+k, 42.62.Fi

I. INTRODUCTION

Magnesium belongs to a small group of atomic species that permit the implementation of a lattice clock. This type of clock relies on the spectroscopy of strongly forbidden transitions of neutral atoms confined in an optical lattice tuned to a wavelength, where the effective dynamic Stark shift of the transition frequency vanished in first order [1]. Lattice clocks have been demonstrated so far for strontium [1] and ytterbium [2]. Recently, lattice clocks based on strontium led the way to accuracies and stabilities beyond current state-of-the-art microwave clocks [3].

The ultimate accuracy of such clocks is currently investigated in many experiments. Each species and isotope shows different advantages and disadvantages especially with respect to systematic errors. A magnesium lattice clock, based on the transition $^1S_0 \rightarrow {}^3P_0$ (see Fig. 1), can be implemented by using an optical lattice at the magic wavelength of around 432 nm [4] and by tailoring the linewidth with an external magnetic field [5]. According to [6] magnesium displays the interesting feature that the blackbody radiation shift of the $^1S_0 \rightarrow {}^3P_0$ transition is the lowest for all earth-alkaline metals and is, e.g., 10 times smaller compared to strontium. This motivates research directed to implement such a clock.

In contrast to strontium, where the absolute frequency of the intercombination transition was known from thermal beam measurements [7,8], comparable data are not available for magnesium. The wavelength of the transition $^1S_0 \rightarrow {}^3P_1$ was measured by grating spectroscopy [9] with a relative accuracy of 10^{-6}. Precise measurements of the fine structure of the metastable states $^3P_{0,1}$ were performed by Godone and Novero [10].

In this paper we present an absolute frequency measurement of the $(3s^2)^1S_0 \rightarrow (3s3p)^3P_1$ intercombination line in magnesium with thermal atoms. In the case of magnesium the frequency of the transition $(3s^2)^1S_0 \rightarrow (3s3p)^3P_0$ can be derived by a combination of this measurement with the measurement of the fine structure. The frequency values of the intercombination transitions for various magnesium isotopes are determined and can be used as an anchor for future precision frequency measurements based on cold atoms in a lattice.

This paper is organized as follows: Section II describes the experimental setup including the stabilized diode laser, the atomic beam apparatus, and the fiber laser frequency comb. In Sec. III we present the results of the absolute frequency measurement of the magnesium intercombination transition as well as an investigation of the stability of this frequency standard. Finally, we discuss in detail the main contributions to the uncertainty of our frequency measurement in Sec. IV.

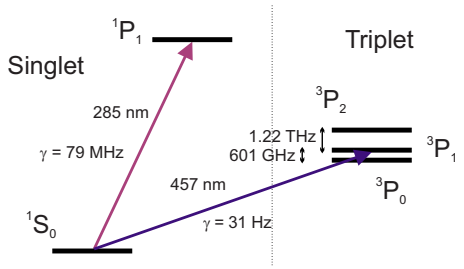

FIG. 1. (Color online) Level scheme for ^{24}Mg displaying the typical features of neutral atom optical frequency standards such as a strong cooling transition and a narrow intercombination line.

*friebe@iqo.uni-hannover.de

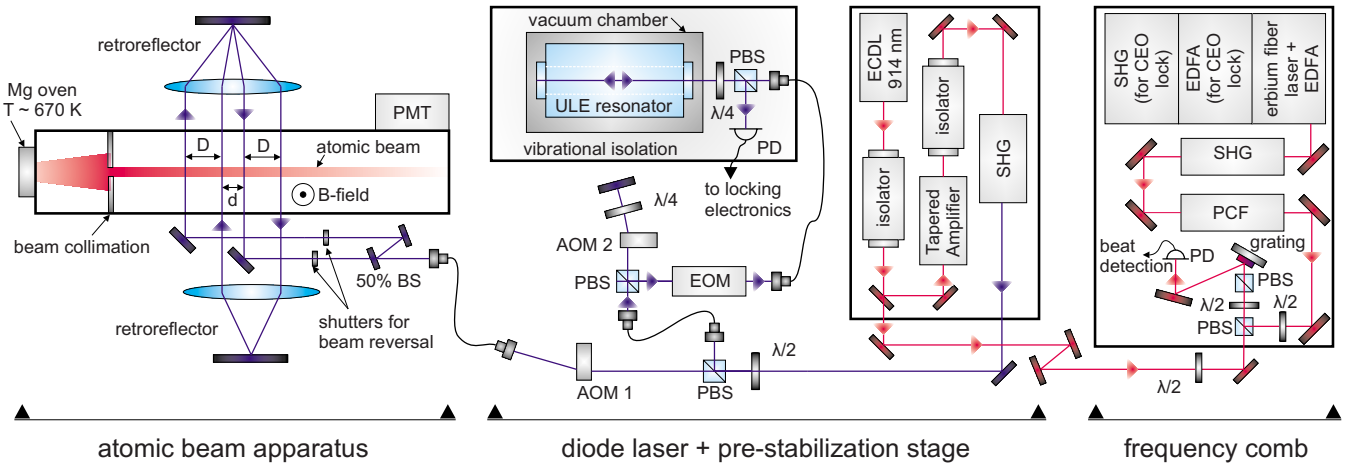

FIG. 2. (Color online) Setup of the magnesium optical frequency standard consisting of a stabilized diode laser system, an atomic beam apparatus, and a commercial femtosecond fiber laser. EOM, electro-optic modulator; PD, photodetector; PBS, polarized beam splitter; BS, beam splitter; PCF, photonic-crystal fiber

II. EXPERIMENTAL SETUP

A. Stabilized diode laser

The laser system used for interrogation of the magnesium clock transition is based on the commercially available TA-SHG 110 (Toptica Photonics). It consists of an extended cavity diode laser (ECDL) in Littrow configuration, a tapered amplifier, and a resonant second harmonic generation (SHG) in bow-tie configuration with a $KNbO_3$ crystal. A small amount of the diode laser's light is picked up behind a deflection mirror and sent to the optical frequency comb for measurement purposes. Typically, this system delivers an output power of about 220 mW at 457 nm. The laser is locked to a 160-mm-long high-finesse ($\mathcal{F}=39\,000$) cavity made of ultralow-expansion (ULE) material. This is mounted in a vacuum chamber on a granite block suspended from the ceiling for efficient suppression of acoustical and mechanical noise. The maximum observed drift of the laser frequency over several minutes is ± 3 Hz/s. Further details of our ULE cavity setup can be found elsewhere [11]. The error signal for the stabilization is obtained by the Pound-Drever-Hall (PDH) technique [12]: A small amount of the blue light is transferred via a polarization maintaining single-mode (pm) fiber to the suspended cavity platform as shown in Fig. 2 where the laser light is phase modulated by an EOM operated at a frequency of 9.7 MHz. An additional double-pass acousto-optic modulator (AOM) allows for frequency tuning. The PDH stabilization is accomplished via feedback to the laser diode current and the laser cavity piezoelectric transducer (PZT). To evaluate the linewidth of our laser system we performed a beat-note measurement with a dye laser with a linewidth of about 870 Hz after stabilization to a Zerodur cavity [11]. Figure 3 shows a beat-note linewidth of 1 kHz, which gives an upper limit for the linewidth of our spectroscopy laser at the second harmonic wavelength.

B. Atomic-beam apparatus

The magnesium clock is based on a thermal atomic-beam Ramsey-Bordé apparatus. The collimated atomic beam has an average velocity of about 900 m/s. In our case the interferometer is realized with two pairs of antiparallel traveling light waves perpendicular to the atomic beam [13] as shown in Fig. 2. The interaction region is enclosed by magnetic shielding. Small angular mismatch between the four beams leads to a reduction of contrast and introduces phase shifts in the interference pattern. Parallel preparation of all four laser beams is realized by means of two cat's eye retroreflectors [14], each consisting of a mirror and a lens separated by the focal length of $f=400$ mm. A pm fiber delivers the light to the beam apparatus and acts as a spatial mode filter that generates a nearly perfect Gaussian beam profile. We have applied a constant magnetic field of $B=6.77\times 10^{-5}$ T to lift the degeneracy of the Zeeman sublevels.

The resolution of such an interferometer is only determined by the propagation time of the atoms between the copropagating laser beams. The separation of the laser beams is adjusted to $D\cong 4.5$ mm such that the signals of the two atom interferometers simultaneously formed in the Ramsey-Bordé scheme add up constructively. Figure 4 shows an interference pattern obtained with our apparatus by scanning the frequency of the laser across the resonance. The atoms

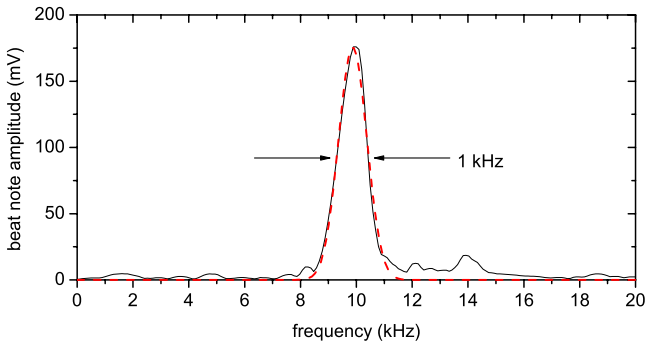

FIG. 3. (Color online) Beat note measurement at 457 nm between the stabilized diode and dye laser with a linewidth of about 870 Hz. Resolution bandwidth: 1 kHz, sweeptime 45 ms. Red dashed line: Gauss fit with full width at half maximum (FWHM) of 1 kHz.

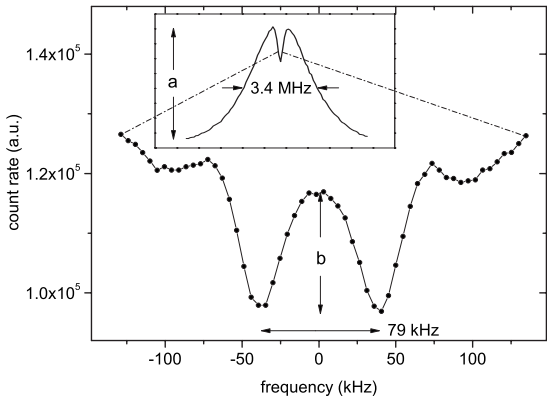

FIG. 4. Typical interference pattern observed with our apparatus. The averaging time per point is 2 s. The inset shows the complete spectrum on a larger frequency scale. We obtained a contrast of the interference pattern of $b/a=12\%$, which was limited by the maximum optical power of about 30 mW available at the experiment.

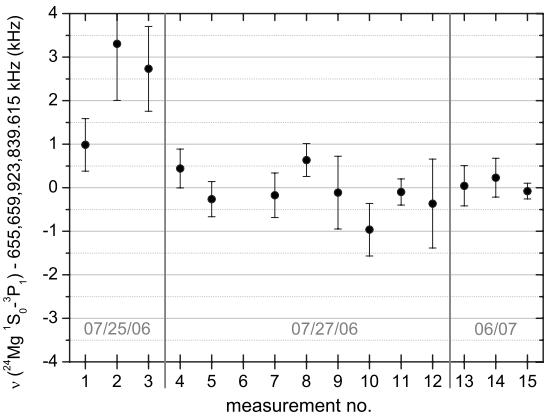

FIG. 5. Measurement results corrected for systematics with respect to the weighted average of all relevant values. Error bars only account for statistical measurement uncertainties.

excited in the interferometer to the state $|^3P_1, m_J=0\rangle$ are measured by detection of the fluorescence of the atoms decaying to the ground state with a photomultiplier tube (PMT). Further details of this apparatus can be found elsewhere [15].

Frequency stabilization of our spectroscopy laser to the central fringe of the resonance is realized by a computer-controlled square-wave modulation of the laser frequency. The interferometer is operated with this technique alternatingly at both sides of the central fringe. The error signal is deduced by subtracting the different PMT counts at the two points from each other. The modulation is performed using an AOM 1, operated near 80 MHz in negative first order of diffraction. The digitally processed error signal serves to correct the offset frequency between the laser and ULE cavity generated by AOM 2. To avoid offset drifts the AOM drivers are referenced to the primary frequency standard.

C. Frequency comb

We use the optical frequency synthesizer FC1500 (Menlo Systems) to generate the optical frequency comb spectrum [16]. The laser source of the FC1500 is a passively mode-locked femtosecond fiber laser [17] which operates at a center wavelength of approximately 1550 nm and has a repetition rate of 100 MHz. The laser resonator has a small free-space section with one end mirror mounted on a translation stage controlled by a stepper motor. This permits the repetition rate to be tuned over approximately 400 kHz, with finer adjustments being achieved using a PZT.

The output power from the mode-locked laser is split and fed to two independent erbium-doped fiber amplifiers (EDFAs). The output from the first EDFA is broadened using a nonlinear fiber to span the wavelength range from approximately 1000 nm to 2100 nm. This provides the octave-spanning spectrum required for detection of the carrier-envelope offset frequency ν_{ceo} using the self-referencing technique. The $f:2f$ interferometer is set up in a collinear single-arm configuration and uses a periodically poled lithium niobate (PPLN) crystal to frequency double 2100 nm radiation to 1050 nm. After the PPLN crystal an interference filter selects out a narrow band of the spectrum around 1050 nm, resulting in a beat signal with a typical signal-to-noise ratio of 40–45 dB. The offset frequency is stabilized by feedback to the pump laser diode current.

A second EDFA generates high-power radiation which is frequency doubled using a PPLN crystal, generating a narrow-band frequency comb around 780 nm. This is subsequently broadened in a nonlinear fiber to generate a comb spanning the range 580–940 nm. This second comb output is used to observe heterodyne beat signals with the fundamental frequency of our spectroscopy laser at 914 nm.

III. SPECTROSCOPIC RESULTS

We have determined the transition frequency of the magnesium intercombination line $(3s^2)^1S_0 \rightarrow (3s3p)^3P_1$ with respect to a portable Cs atomic clock (HP 5071A high performance, relative accuracy: $\pm 2.0\times 10^{-13}$, relative instability: $\leqslant 5.0\times 10^{-12}$ in 1 s) from the Physikalisch-Technische Bundesanstalt (PTB). Frequency measurements were performed in July 2006 on two different days and repeated in June 2007. Each time the interferometer was carefully realigned. The results are shown in Fig. 5. Each data point is the arithmetic mean value of two frequency measurements, which were obtained by reversing the laser beams of the Ramsey-Bordé interferometer. Notice that proper alignment of the beam reversal was not ensured in measurement Nos. 2 and 3 and these values have therefore been neglected for the determination of the average transition frequency. Measurement Nos. 7 and 8 show the effect of reduced excitation intensity. In these experiments the optical power has been reduced to approximately 30% and 60%, respectively. Since a reduced intensity leads to a change in excitation probability for different velocity classes, it consequently directly affects the second-order Doppler shift (see also Sec. IV B), and for this reason the values were also excluded and do not contribute to the average frequency value. To verify the effectiveness of our μ-metal shielding the magnetic offset field has been switched off, inverted, and returned to normal configu-

TABLE I. Shifts and uncertainties of the frequency measurement.

Contribution	Shift[a] (Hz)	Uncertainty (Hz)	Relative uncertainty
Line shift[b]	−1641.1	1612	2.5×10^{-12}
Cs clock	0	131	2.0×10^{-13}
Statistical uncertainty	0	120	1.8×10^{-13}
Total	−1641.1	1622	2.5×10^{-12}

[a] $\nu_{shift}=\nu_{observed}-\nu_{magnesium}$.
[b] Discussed in Sec. IV.

ration in measurement Nos. 10–12. Measurement Nos. 13–15 were recorded approximately 1 year after the first measurement run and are in good agreement with the other frequency values.

The absolute frequency values in Fig. 5 can be calculated according to

$$\nu(^1S_0 \rightarrow {}^3P_1) = 2(2\nu_{ceo} + mf_{rep} + \nu_{fx}) - 80\ \text{MHz}, \quad (1)$$

where ν_{fx} is the beat note between diode laser and femtosecond laser at 914 nm and the offset of −80 MHz is included due to AOM 1 (see Fig. 2). The mode number m of the fiber comb has been determined in two different ways: As a first anchor for our target frequency we have calibrated our high-precision wavelength meter (high-finesse WS Ultimate, 40 MHz accuracy) with an iodine-stabilized He-Ne laser and shortly afterwards measured the frequency of the magnesium intercombination line. In a second experiment we applied a method proposed by Holzwarth *et al.* [18], where the mode number m was determined for different repetition rates f_{rep} and fixed laser frequency by applying Eq. (1).

Table I summarizes the uncertainty contributions to the measurement of the magnesium intercombination line. The weighted average of all considered measurements has been determined to be

$$\nu(^{24}\text{Mg}\ ^1S_0 \rightarrow {}^3P_1) = 655\,659\,923\,839.6\ (1.6)\ \text{kHz}, \quad (2)$$

corresponding to a wave number of approximately 21 870.4609 cm^{-1}. This value is in good agreement with, to our knowledge, the most recent published value in [9] where a wave number of 21 870.464 (0.02) cm^{-1} has been determined in a measurement based on grating spectrometry which dates back to 1965. Compared to this result we have decreased the measurement uncertainty of the magnesium intercombination line frequency by six orders of magnitude. In a previous experiment which was performed in 1938 Meißner [19] obtained a wave number of 21 870.484 cm^{-1}. This value deviates approximately 700 MHz from our result. Our measured frequency can be used as an anchor to calculate the other optical transitions from $^1S_0$ into the ^3P_J level system with the help of the well-known radio-frequency transitions in the triplet system as shown in Table II.

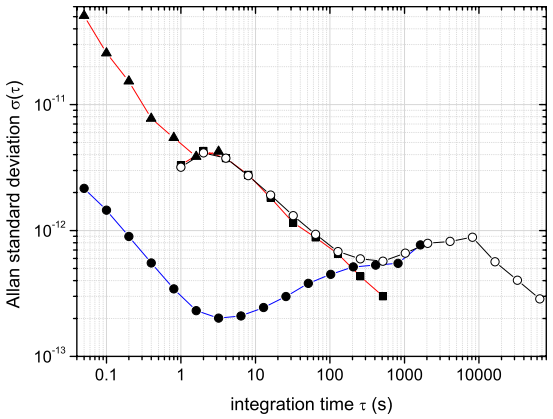

FIG. 6. (Color online) Allan standard deviation of our frequency standard with respect to a quartz oscillator (solid circles, blue) and with respect to a portable Cs clock (solid squares and triangles, red). Open circles: Cs clock vs GPS-disciplined quartz.

The stability of our frequency standard has been characterized with respect to a GPS-disciplined quartz oscillator (Oscilloquartz OCXO 8607 Option 20) and the portable Cs atomic clock. The result is shown in Fig. 6. The instability of the magnesium frequency standard and the quartz is about 3×10^{-13} in 1 s. The instability of the quartz is specified to 2×10^{-13} in 1 s. At integration times less than 100 s the stability measurement against the quartz oscillator sets an upper limit for the instability of the magnesium frequency standard. All absolute frequency measurements have been performed with respect to the Cs clock since the GPS-disciplined quartz reaches an accuracy better than 10^{-12} only for averaging times longer than 10 000 s.

The stability of our Ramsey-Bordé interferometer is investigated with the help of our prestabilized clock laser. For this purpose we recorded an interference pattern (Fig. 4) and subtracted a parabolic curve to remove the incoherent background. Subsequently a cosine term with gaussian amplitude and slightly varying period was fitted to the resulting signal and subtracted. We calculated the Allan deviation $\sigma^{(I)}$ of the

TABLE II. Selection of optical transitions from $^1S_0$ to the ^3P_J level system, calculated from experimental data.

Isotope	Upper level	Shift (relative to $^{24}\text{Mg}\ ^3P_1$)	Absolute transition frequency ($^1S_0 \rightarrow {}^3P_J$)
^{24}Mg	$^3P_0$	−601 277 157 869.1 (0.6) Hz [10]	655 058 646 681.7 (1.6) kHz
^{24}Mg	$^3P_2$	1 220 575.1 (33) MHz [20]	656 880 498.9 (33) MHz
^{25}Mg	$^3P_1$ ($F=7/2$)	1040.7 (0.1) MHz [21]	655 660 964.5 (0.1) MHz
^{25}Mg	$^3P_1$ ($F=5/2$)	1556.8 (0.1) MHz [21]	655 661 480.6 (0.1) MHz
^{25}Mg	$^3P_1$ ($F=3/2$)	1906.8 (0.1) MHz [21]	655 661 830.6 (0.1) MHz
^{26}Mg	$^3P_1$	2683.18 (0.02) MHz [21]	655 662 607.02 (0.02) MHz

residual differences and estimated the Allan deviation $\sigma^{(\nu)}$ according to [22] via

$$\sigma^{(\nu)} = \frac{1}{\partial_\nu I}\sigma^{(I)}, \tag{3}$$

with $\partial_\nu I$ denoting the first derivative of the Ramsey structure taken at the point used for stabilization. Thus, we obtained a relative Allan standard deviation of $\sigma_y(1\ \mathrm{s}) = 6 \times 10^{-13}$. This result is larger than the measured Allan standard deviation between the quartz oscillator and the diode laser which is locked to the Ramsey-Bordé interferometer for longer integration times (see Fig 6).

IV. SYSTEMATIC UNCERTAINTIES

A. Residual first-order Doppler effect

Ideally Ramsey-Bordé spectroscopy strongly suppresses the first-order Doppler effect. Small imperfections of the interrogating beams or defocused retroreflectors can induce residual shifts and phase errors in the interference pattern. Moreover, due to unavoidable aberration in the retroreflector lenses, perfect parallelism can only be obtained for three of the four beams. Studies in [23] showed that small deviations of a few microradians can lead to frequency shifts in the kHz range. Frequency shifts due to phase errors in the excitation zones can be identified, for example, by inverting the propagation direction of the excitating beam, which results in a change of sign of the frequency shift induced by these effects. The arithmetic mean of the forward-running beam measurement and the inverted beam measurement should reveal the correct transition frequency as has been pointed out by Kersten *et al.* [24].

The beam reversal is implemented with a 50% BS in front of the interaction zone. Both Ramsey-Bordé interferometers are carefully aligned such that the laser beams are perfectly overlapped and travel equal distances. The overlap of the laser beams for the two interferometer configurations with reversed laser beams was optimized along several meters at different points.

The Ramsey-Bordé interferometry was optimized by individually adjusting the retroreflecting units. The first unit was aligned according to the procedure proposed in [25] with the help of saturation spectroscopy. The second retroreflector unit was aligned by optimizing the contrast of the interference pattern.

We investigated if the beam-reversal technique cancels systematic frequency shifts caused by misalignment of the second reflector unit. For this purpose we used our ULE resonator as a short-term frequency reference. The result is shown in Fig. 7 where a linear drift of the resonator has been subtracted. The mean frequency resulting from the beam reversal does not show any systematics with respect to the defocusing of the retroreflecting mirror. The maximum frequency difference of $\Delta\nu \approx 1400$ Hz observed in this set of measurements was taken as a rough estimate for the upper limit of the error due to the residual Doppler effect also in the case of the optimized Ramsey-Bordé interferometer.

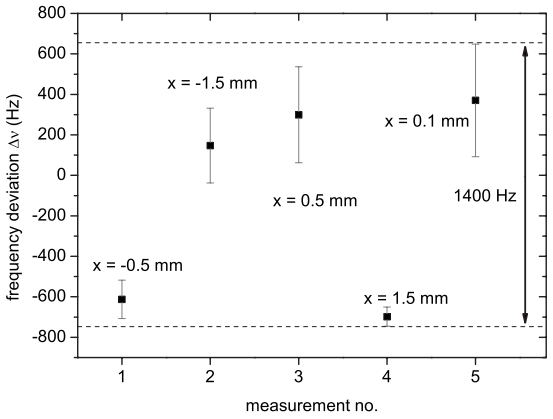

FIG. 7. Frequency deviation for different displacements (x) of one cat's eye mirror from optimal position.

B. Second-order Doppler effect

The Ramsey-Bordé interferometer cancels the Doppler effect only in first order of v/c. For thermal atomic beams with velocities of several hundred m/s, the quadratic term is of the order of a few kHz for transition frequencies in the optical domain, corresponding to a relative frequency uncertainty of 10^{-12}. The estimation of the second-order Doppler effect follows [24], where the experimentally observed interference pattern is compared with a calculated interference pattern without the term of the second-order Doppler effect. The experimental interference pattern can be expressed by

$$I(\Delta) = \int_0^\infty dv\, g(v)\left\{\cos\left(\frac{2D}{v}\left[\Delta + \omega_0\frac{v^2}{2c^2} + \frac{\hbar k^2}{2m}\right]\right) + \cos\left(\frac{2D}{v}\left[\Delta + \omega_0\frac{v^2}{2c^2} - \frac{\hbar k^2}{2m}\right]\right)\right\}, \tag{4}$$

where the cosine terms represent the Ramsey signals of atoms passing the interaction zones (distance D) with velocity v. $\Delta := \omega - \omega_0$ is the detuning of the interrogating light with frequency $\omega = ck$. $g(v)$ is a velocity-dependent weighting factor which accounts for thermal velocity-distribution of the atoms and the complex dependences of the excitation and detection probability on the atomic velocity. In order to calculate the interference signal without the second-order Doppler effect, the weighting factor $g(v)$ has to be determined. This can be done to sufficient approximation by Fourier transformation of $I(\Delta)$:

$$\tilde{I}(t) = \frac{D}{t^2}g\left(\frac{2D}{t}\right)(e^{it\hbar k^2/2m} + e^{-it\hbar k^2/2m})$$
$$\Leftrightarrow g\left(\frac{2D}{t}\right) = \frac{t^2}{2D\cos\left(t\frac{\hbar k^2}{2m}\right)}\tilde{I}(t). \tag{5}$$

For the Fourier transform the second-order Doppler effect is neglected. The modified interference signal without the second-order Doppler effect is given by

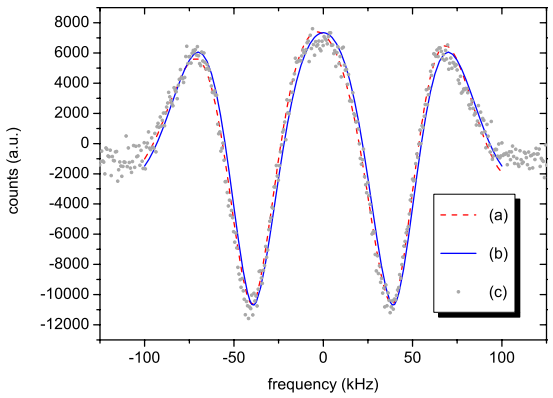

FIG. 8. (Color online) Theoretical Ramsey fringes with (a) and without a second-order Doppler shift (b) calculated from experimental parameters; (c) shows the experimental data points.

$$I(\Delta) = D\int_{-\infty}^{\infty} dt\, g\left(\frac{2D}{t}\right)\frac{1}{t^2}(e^{it\hbar k^2/2m} + e^{-it\hbar k^2/2m})e^{it\Delta}, \quad (6)$$

where we performed the substitution $t=2D/v$.

We fitted a second-degree polynomial to the Lamb dip of our experimental data and subtracted it from the Ramsey fringes to eliminate the incoherent background. With the known distribution function $g(v)$ we were able to calculate the Ramsey fringes from Eq. (4) for the case with and without a second-order Doppler shift. The quality of the approximation is tested by reinserting the evaluated velocity weighting factor in (4) and by comparing the resulting signal with experimental data. As shown in Fig. 8, the deviation is negligible compared to other uncertainties related to this effect such as knowledge of D. We calculated the whole fringe pattern as shown in Fig. 8 and determined due to our laser-locking scheme (Sec. II B) the shift on the sides of the central fringe and obtained a second-order Doppler shift of $\Delta\nu = -1643$ Hz.

In order to estimate the influence of the uncertainty of D we calculated the second-order Doppler effect for $D = 3.5-6$ mm. From this we derived a maximum deviation of ± 800 Hz. These results are in good agreement with the experimentally determined value of -1.5 (0.4) kHz by [26].

C. External fields

The presence of a small static electric field inside the atomic-beam apparatus (caused, for example, by terrestrial stray fields and nonperfect conducting properties of the vacuum chamber materials) leads to a shift of atomic energy levels due to the Stark effect. The difference of the polarizabilities of the $^1S_0$ and $^3P_1$ states was experimentally determined in [27] as $\Delta\alpha = \alpha(^3P_1, m=0) - \alpha(^1S_0) = 3.9$ (0.1) kHz $(\mathrm{cm/kV})^2$. With $\Delta\nu = -\frac{1}{2}\Delta\alpha E^2$ and the assumption for the electrostatic rest field E to be 5 (5) V/cm we estimate a line shift of $\Delta\nu = -0.05$ (0.05) Hz.

The $^1S_0 \rightarrow {}^3P_1$ $(m_J=0)$ transition shows no first-order Zeeman shift. However, this shift no longer vanishes in second or higher orders of B. The correction term $E_n^{(2)}$ of the nth energy level $E_n = \Sigma_{i=0}^{\infty} E_n^{(i)}$ in second-order stationary perturbation theory has the form

$$E_n^{(2)} = \sum_{m\neq n} \frac{|\langle m^{(0)}|\hat{H}_I|n^{(0)}\rangle|^2}{E_n^{(0)} - E_m^{(0)}}, \quad (7)$$

where $|n^{(0)}\rangle$, $E_n^{(0)}$ is the unperturbed nth state and energy level, respectively, and the sum runs over all unperturbed states. $\hat{H}_I$ is the interaction Hamiltonian and in the case of a static homogeneous magnetic field B (chosen to be in the direction of the z axis) given by

$$\hat{H}_I = \frac{e}{2m_e}(\hat{L}_z + g_s\hat{S}_z)B_z, \quad (8)$$

where $\hat{L}_z$ and $\hat{S}_z$ are the operators of angular momentum and electronic spin, e the elementary charge, m_e the electron mass, and $g_s \approx 2$ the Landé factor. As the $^1S_0$ state stays unshifted, we have to take into account only the $^3P_1$ state. The correction terms are proportional to the inverse difference of the energy levels, so only the $^3P_0$ and $^3P_2$ states with $\nu_{^3P_1 \rightarrow {}^3P_0} = 601$ GHz and $\nu_{^3P_2 \rightarrow {}^3P_1} = 1.22$ THz contribute significantly to the sum in (7). All other energy levels (with transition frequencies to $^3P_1$ of more than a few hundred THz) can be neglected. By use of the Clebsch-Gordan coefficients we write the atomic $|J,m_J\rangle$ eigenstates as $|L,m_L\rangle \otimes |S,m_S\rangle$ eigenstates of the $\hat{L}_z$ and $\hat{S}_z$ operators, evaluate the sum in (7), and arrive at

$$E_{^3P_1}^{(2)} = \frac{1}{3}\left(\frac{e\hbar B}{2m}\right)^2\left[\frac{2}{E_{^3P_1}^{(0)} - E_{^3P_0}^{(0)}} - \frac{1}{E_{^3P_2}^{(0)} - E_{^3P_1}^{(0)}}\right]. \quad (9)$$

Therefore, the shift $\Delta\nu$ of the transition frequency can be written after evaluating Eq. (9) with the numerical values as

$$\Delta\nu = 1.64 \times 10^8 \frac{\mathrm{Hz}}{\mathrm{T}^2} \times B^2. \quad (10)$$

By measuring the linear Zeeman shift of the $^3P_1$ $(m_J = -1, m_J = 1)$ substates we determined the strength of the applied homogeneous magnetic field to be $B = 6.77$ (0.45) $\times 10^{-5}$ T. This causes a shift in second order of $\Delta\nu = 0.75$ (0.1) Hz far below the accuracy of our apparatus.

D. Sagnac effect

The thermal beam Ramsey-Bordé interferometer is sensitive to rotations. The resulting frequency shift can be calculated [28] as

$$\Delta\nu = \frac{\Omega(D+d)}{\lambda}, \quad (11)$$

with λ the wavelength of the interrogating light and D the distance between the copropagating and d between the counterpropagating beams (Fig. 2). With values of $D = 4.5$ (1.0) mm, $d = 5.0$ (1.0) mm, and a rotation of the apparatus of $\Omega = 5.75 \times 10^{-5}$ s^{-1}, which is caused by revolution of the Earth, we derive a frequency shift of $\Delta\nu = 1.2$ (0.1) Hz.

Table III summarizes all relevant uncertainty contributions to the line shift of the magnesium frequency standard.

TABLE III. Shifts and uncertainties of the ^{24}Mg $(3s^2)^1S_0 \rightarrow (3s3p)^3P_1$ transition measured on a thermal atomic beam.

Effect	Shift (Hz)	Uncertainty (Hz)	Relative uncertainty
First-order Doppler	0	1400	2.1×10^{-12}
Second-order Doppler	−1643	800	1.2×10^{-12}
External magnetic field	0.75	0.1	1.5×10^{-16}
External electric field	−0.05	0.05	7.5×10^{-17}
Sagnac effect	1.2	0.1	1.5×10^{-16}
Total	−1641.1	1612	2.5×10^{-12}

V. CONCLUSION AND OUTLOOK

An optical frequency standard based on neutral magnesium has been realized. We determined the frequency of the intercombination line $^1S_0 \rightarrow {}^3P_1$ at 457 nm with an accuracy of 2.5×10^{-12}. Our result deviates by 70 MHz from a value obtained by Risberg [9] in 1965 which is a tenth of the quoted error and differs by 700 MHz from a previous measurement performed by Meißner in 1938. We used the measured frequency to calculate optical transitions from $^1S_0$ into the ^3P_J level system (Table II). Especially the $^1S_0 \rightarrow {}^3P_0$ transition is interesting for future applications such as an optical lattice clock with magnesium.

By application of the beam-reversal technique we were able to reduce one of the main uncertainty contributions in Ramsey-Bordé interferometry on thermal atoms, the residual first-order Doppler effect, to a level of 2.1×10^{-12}. The residual linear and second-order Doppler effects limit the achieved uncertainty of our frequency standard. A further considerable enhancement in accuracy can only be expected from measurements on laser-cooled free-falling atoms or in dipole-trap-captured atoms in combination with a primary frequency reference with superior stability compared to the presently used Cs clock. Currently we are investigating possible experimental strategies [29–31] to implement a lattice clock, which is expected to improve the current uncertainty in accuracy by several orders of magnitude.

ACKNOWLEDGMENTS

This work was supported by the Deutsche Forschungsgemeinschaft (DFG) under Grant No. SFB 407. The authors would like to thank Andreas Bauch from the PTB for providing a portable Cs atomic clock.

[1] M. Takamoto, F.-L. Hong, R. Higashi, and H. Katori, Nature (London) **435**, 321 (2005).
[2] N. Poli *et al.*, Phys. Rev. A **77**, 050501(R) (2008).
[3] A. D. Ludlow, T. Zelevinsky, G. K. Campbell, S. Blatt, M. M. Boyd, M. H. G. de Miranda, M. J. Martin, J. W. Thomsen, S. M. Foreman, J. Ye *et al.*, Science **319**, 1805 (2008).
[4] V. D. Ovsiannikov, V. G. Pal'chikov, A. V. Taichenachev, V. I. Yudin, H. Katori, and M. Takamoto, Phys. Rev. A **75**, 020501(R) (2007).
[5] A. V. Taichenachev, V. I. Yudin, C. W. Oates, C. W. Hoyt, Z. W. Barber, and L. Hollberg, Phys. Rev. Lett. **96**, 083001 (2006).
[6] S. G. Porsev and A. Derevianko, Phys. Rev. A **74**, 020502(R) (2006).
[7] G. Ferrari, P. Cancio, R. Drullinger, G. Giusfredi, N. Poli, M. Prevedelli, C. Toninelli, and G. M. Tino, Phys. Rev. Lett. **91**, 243002 (2003).
[8] I. Courtillot, A. Quessada-Vial, A. Brusch, D. Kolker, G. Rovera, and P. Lemonde, Eur. Phys. J. D **33**, 161 (2005).
[9] G. Risberg, Ark. Fys. **28**, 381 (1965).
[10] A. Godone and C. Novero, Metrologia **30**, 163 (1993).
[11] J. Keupp, A. Douillet, T. E. Mehlstäubler, N. Rehbein, E. M. Rasel, and W. Ertmer, Eur. Phys. J. D **36**, 289294 (2005).
[12] R. W. P. Drever, J. L. Hall, F. V. Kowalski, J. Hough, G. M. Ford, A. J. Munley, and H. Ward, Appl. Phys. B: Photophys. Laser Chem. **31**, 97 (1983).
[13] C. J. Bordé, C. Salomon, S. Avrillier, A. VanLerberghe, C. Bréant, D. Bassi, and G. Scoles, Phys. Rev. A **30**, 1836 (1984).
[14] J. J. Snyder, Appl. Opt. **14** (1975).
[15] H. Hinderthür, A. Pautz, V. Rieger, F. Ruschewitz, J. L. Peng, K. Sengstock, and W. Ertmer, Phys. Rev. A **56**, 2085 (1997).
[16] P. Kubina, P. Adel, F. Adler, G. Grosche, T. W. Hänsch, R. Holzwarth, A. Leitenstorfer, B. Lipphardt, and H. Schnatz, Opt. Express **13**, 904 (2005).
[17] K. Tamura, E. P. Ippen, H. A. Haus, and L. E. Nelson, Opt. Lett. **18**, 1080 (1993).
[18] R. Holzwarth *et al.*, Appl. Phys. B: Lasers Opt. **73**, 269271 (2001).
[19] K. W. Meißner, Ann. Phys. **5**, 505 (1938).
[20] M. Inguscio, K. R. Leopold, J. S. Murray, and K. M. Evenson, J. Opt. Soc. Am. B **2**, 1566 (1985).
[21] U. Sterr, K. Sengstock, J. H. Müller, and W. Ertmer, Appl. Phys. B: Photophys. Laser Chem. **56**, 62 (1993).
[22] F. Riehle, *Frequency Standards* (Wiley-VCH, Berlin, 2004).
[23] K. Sengstock, U. Sterr, J. H. Müller, V. Rieger, D. Bettermann, and W. Ertmer, Appl. Phys. B: Lasers Opt. **59**, 99 (1994).
[24] P. Kersten, F. Mensing, U. Sterr, and F. Riehle, Appl. Phys. B: Lasers Opt. **68**, 27 (1999).
[25] A. Morinaga, F. Riehle, J. Ishikawaa, and J. Helmcke, Appl. Phys. B: Photophys. Laser Chem. **48**, 165 (1989).
[26] K. Sengstock, U. Sterr, G. Hennig, D. Bettermann, J. H. Müller, and W. Ertmer, Opt. Commun. **103**, 73 (1993).
[27] V. Rieger, Ph.D. thesis, Universität Hannover, 1996.
[28] F. Riehle, T. Kisters, A. Witte, J. Helmcke, and C. J. Bordé, Phys. Rev. Lett. **67**, 177 (1991).
[29] N. Malossi, S. Damkjaer, P. L. Hansen, L. B. Jacobsen, L. Kindt, S. Sauge, J. W. Thomsen, F. C. Cruz, M. Allegrini, and E. Arimondo, Phys. Rev. A **72**, 051403(R) (2005).
[30] T. E. Mehlstäubler, K. Moldenhauer, M. Riedmann, N. Rehbein, J. Friebe, E. M. Rasel, and W. Ertmer, Phys. Rev. A **77**, 021402(R) (2008).
[31] T. Binnewies, G. Wilpers, U. Sterr, F. Riehle, J. Helmcke, T. E. Mehlstäubler, E. M. Rasel, and W. Ertmer, Phys. Rev. Lett. **87**, 123002 (2001).